Plasma Chemistry and Plasma Processing (2019) 39:667–682
https://doi.org/10.1007/s11090-019-09971-y

ORIGINAL PAPER

About the Development and Dynamics of Microdischarges in Toluene-Containing Air

Ronny Brandenburg[1,2] · Sina Jahanbakhsh[1] · Milko Schiorlin[1] · Michael Schmidt[1]

Received: 7 December 2018 / Accepted: 4 March 2019 / Published online: 15 March 2019

Abstract
The development of microdischarges and the inception dynamics of subsequent microdischarges in an electrode arrangement consisting of a metal pin and a hemispherical dielectric-covered electrode, operated in air with a small toluene admixture, is studied. The discharge is operated with sinusoidal high voltage. A gated ICCD camera and a current probe enable the recording of images and current pulses of the single microdischarges, respectively, while the spatio-temporally resolved development is measured with a multi-dimensional time-correlated single photon counting technique. The overall discharge dynamics changes significantly if a concentration of 35 ppm toluene is added to dry air. A lower high voltage amplitude than in dry air is needed for stable discharge operation. This can be explained by the lower ionization energy of toluene compared to molecular oxygen and nitrogen. The microdischarge development is the same with or without admixture, i.e. a positive (cathode directed) streamer mechanism is observed. Lower mean power is dissipated into the discharge when toluene is admixed. The main effect caused by toluene admixture is the suppression of high-energy microdischarges in case of the cathodic pin half-cycle of the sinusoidal high voltage. The influence on the inception voltage by additional ionization mechanisms and volume memory effects, the consumption of energetic electrons for toluene decomposition reactions, and the modification of the surface by plasma treatment are discussed as possible reasons.

Keywords Dielectric barrier discharge · Atmospheric pressure plasma · Microdischarge · Pollutant degradation · Volatile organic compounds · Toluene removal

Introduction

Dielectric barrier discharges (DBDs) are an established approach for the generation of ozone and the abatement of air impurities from exhausts and off-gases [1–3]. In particular, the removal of volatile organic compounds (VOCs), specially odorous molecules, was widely studied by plasma and plasma-catalyst combination [3–7]. The conversion of VOCs

✉ Ronny Brandenburg
brandenburg@inp-greifswald.de

[1] Leibniz Institute for Plasma Science and Technology e.V. (INP Greifswald), Greifswald, Germany

[2] Institute of Physics, University of Rostock, Rostock, Germany

in air is mainly via oxidising reactions driven by free radicals such as oxygen atoms O, OH, HO_2, ions and other reactive species, e.g. ozone [5–7]. The conversion, energy efficiency, carbon balance and selectivity to CO_2 are improved when plasma is coupled with a catalyst and undesired by-products such as ozone and solid deposits at walls are suppressed [8, 9].

DBD plasmas are commonly filamentary, i.e. consisting of transient and thin individual microdischarges (MDs) [10–12]. The generation of free radicals and ions via electron-impact dissociation is determined by the mechanisms and basic plasma parameters of the MDs. Microplasmas and its diagnostic are a topic of research since about four decades [10–15]. The physics of MDs or single DBDs in air and other nitrogen/oxygen gas mixtures has been studied by experimental methods, in particular electrical measurements [16–23], optical emission spectroscopy and imaging [24–29], Streak camera recording [19, 30], time-correlated single photon counting [31–33] and laser diagnostics [34–37] as well as by simulation and modelling [38–46]. In [47] the correlation of the chemical reaction pathways for the oxidation of toluene and trichlorethylene with the physical behaviour of MDs was studied. The variation of the oxygen concentration in argon and nitrogen had a significant impact on the removal efficiency, which was explained by the balances between atomic oxygen generation, its fast reactions with the VOC molecules and the formation of ozone, which is slow reacting with the hydrocarbons. Although numerous publications describe the removal of a large variety of hydrocarbons in DBDs, with and without a catalyst (see e.g. [3–7] and references therein), an experimental study dedicated to the MD development in low-level VOC-containing air is still missing. Even small admixtures of VOCs (ppm or sub-ppm level) can cause distinct changes on the discharge dynamics. As an example, it is observed that in case of a defined admixture of about 30 ppm of oxygen to nitrogen even the discharge regime changes from a diffuse or uniform discharge to a filamentary plasma [48]. In addition, the humidity has an effect on both, the discharge physics and the removal efficiency of VOCs [49].

Recently, a metal pin-to-dielectric-covered electrode arrangement was investigated in dry air [50]. This electrode arrangement combines the main features of single-DBDs and corona discharges. It can also be seen as a miniaturization of a DBD stack reactor, i.e. volume DBD arrangements consisting of a stack of dielectric plates (Al_2O_3 or mica) and woven mesh electrodes (fabric made of stainless steel) operated at alternating potential of the high voltage–power supply [51]. The reactor concept has been used to clean air admixed with toluene and other VOCs in the past (e.g. [52]). This work also motivated the study of single MDs in low-level VOC contaminated air.

Toluene ($C_6H_5CH_3$) was chosen as the VOC in this study. It is an aromatic compound and one of the most frequent used hydrocarbon in laboratory studies concerning the VOC removal by means of plasmas or plasma-catalyst combination [5–7]. Furthermore, it is one of the most widespread hydrocarbon in the troposphere since it is extensively used in industry e.g. as a solvent or thinner, in rubber, in cosmetics and in adhesives, as a gasoline additive or for the synthesis of other chemicals. Toluene is hazardous as it affects the central nervous system and is known to cause several illness (e.g. drowsiness, headache, nausea) [5–7].

Experimental Set-Up

The experimental set-up is the same as described in [50] except the gas supply system. Figure 1 sketches the overall set-up. Only the main aspects of the discharge arrangement and the measurement procedure are given in the following.

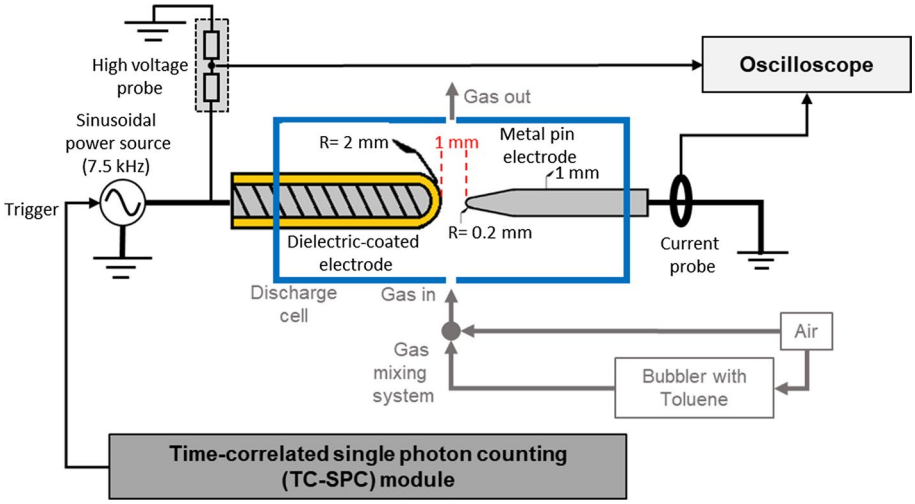

Fig. 1 Scheme of the experimental set-up

The discharge cell is a closed cell made of polycarbonate with two quartz windows. It contains the metal pin electrode as well as the dielectric-covered hemispherical electrode. The latter is a cap made of alumina (Al_2O_3, relative permittivity 9, radius 2 mm) containing the second metal electrode. The thickness of the dielectric at the tip is about 0.5 mm [30]. The gas-gap distance between the electrodes is 1 mm.

The electrodes are aligned horizontally and the gas (dry air plus toluene admixture) is flowing through the cell from the bottom to the top. The gas is prepared by mixing two gas lines controlled with separate mass flow controllers. One line of dry air is kept constant at a flowrate of 300 sccm and the other passes through a bubbler filled with toluene. The gas flow rate though the bubbler is varied from 0 to 4 sccm, but most of the experiments were conducted at 1.5 sccm. The hydrocarbon-containing dry air is admixed with the "pure" dry air gas flow, resulting in a long time stable toluene admixture. The toluene concentration was determined by means of micro-GC analysis (Inficon, 3000 Micro GC).

A sinusoidal voltage at 7.5 kHz (period of 134 µs) is applied to the dielectric-covered hemispherical electrode, while the pin is grounded. The applied voltage amplitude is 11.4 kV_{pp} during all experiments. The diagnostic methods include electrical (current and voltage) measurements, optical (morphology of the discharge by taking ICCD images), and time-correlated single photon counting (TC-SPC, spatio-temporally resolved discharge development). A current probe (Tektronix CT-1, bandwidth: 1 GHz) is surrounding the grounded lead of the metal pin electrode, and a voltage probe (1000:1, Tektronix P6015A) is connected to the high-voltage contact of the dielectric-covered electrode. An oscilloscope (Tektronix DPO4104, bandwidth: 1 GHz, sampling rate: 5 GHz) records current and voltage. The distribution of the current pulses is measured using the "histogram" option of the oscilloscope. For current pulse distribution over the applied voltage cycle "horizontal histogram" option of the oscilloscope is used. Current pulse amplitude distributions are measured using "vertical histogram" option of the oscilloscope. The details of these measurements are described elsewhere [50].

The microdischarges are imaged by a lens, and recorded by an ICCD camera (Andor iStar). By setting the opening of the ICCD gate to different phases of the applied voltage,

it is possible to take images of different discharge events within the high voltage cycle (see [50] for details). To measure the spatio-temporally resolved MD development, the light from the single DBD is guided to a monochromator (Princeton Instrument SP2300) entrance slit. A highly sensitive photomultiplier for single photon counting (Hamamatsu H5773/Becker-Hickl PMC-100-04) is equipped at the exit slit of the monochromator. This photomultiplier is part of the multi-dimensional time-correlated single photon counting (TC-SPC, Becker-Hickl SPC 152) set-up [50]. The high-voltage–power source as well as the diagnostic devices are controlled by a trigger signal generated in the TC-SPC system in order to enable the recording of the MD development for different phases within the applied voltage cycle. The spatial resolution (resolved along the MD axis) is given by imaging and the width of the entrance slit, and it is 25 µm. Technically, the temporal resolution is given by the parameters of the TC-SPC device, namely the time-window of a time-to-amplitude convertor and the number of memory segments covering this time window. It is 12 ps for all experiments (50 ns divided by 4096).

The monochromator enables investigation of different spectral lines or bands emitted by the plasmas. The 0-0 transition of the second positive system (SPS) of nitrogen ($\lambda = 337$ nm), the most intense band of the DBD under the conditions being considered, and the 0-0 transition of the first negative system (FNS) of nitrogen ($\lambda = 391$ nm) are investigated. The dominant excitation process of the radiating states $N_2(C^3\Pi_u)$ and $N_2^+(B^2\Sigma_u^+)$ is direct electron collision with energy thresholds of 11.03 and 18.70 eV, respectively. The main loss processes of the excited molecules are spontaneous emission (according to the radiative lifetime of the state) and collisional quenching by nitrogen and oxygen molecules. For the $N_2^+(B)$ state three-body quenching with nitrogen molecules has to be considered as well. Due to atmospheric pressure the effective lifetimes of the states in dry air are orders of magnitude lower than their radiative lifetimes, namely about 0.6 ns ($N_2(C^3\Pi_u)$ state) and 0.05 ns ($N_2^+(B^2\Sigma_u^+)$ state). A comprehensive overview about lifetimes and quenching coefficients for the calculation of effective lifetimes is given in [53]. A detailed sensitivity analysis including 617 elementary processes performed in [54] revealed that the above mentioned processes are the most dominant and sufficient to describe the radiation kinetics in weakly ionised atmospheric pressure plasmas in dry air. Due to the much higher excitation energy of $N_2^+(B^2\Sigma_u^+)$ the FNS emission is an indicator the development of the electric field strength, while SPS emission is interpreted as a convolution of the electric field strength and the local electron density [31–33, 54].

Results and Discussion

Microdischarge Morphology and Development

The Fig. 2 shows oscillograms of the applied voltage (blue curve) and discharge current (purple lines) after accumulation over 1 s, i.e. 7500 voltage cycles.

An oscillogram (voltage and current development) for dry air is shown in Fig. 2 a. For the negative half-cycle, i.e. the grounded pin acts as the anode, two subsequent MDs per single half-cycle are observed forming two “groups” in the accumulated oscillogram. In the positive half-cycle, i.e. the grounded pin acts as the cathode, an erratic behaviour in terms of the current pulse amplitude and the inception phase is obtained. MDs with amplitudes above 400 mA, but also weaker current pulses are observed. This behaviour is not changing up to a toluene-containing gas flow of 1.5 sccm. For this admixture (see Fig. 2 b),

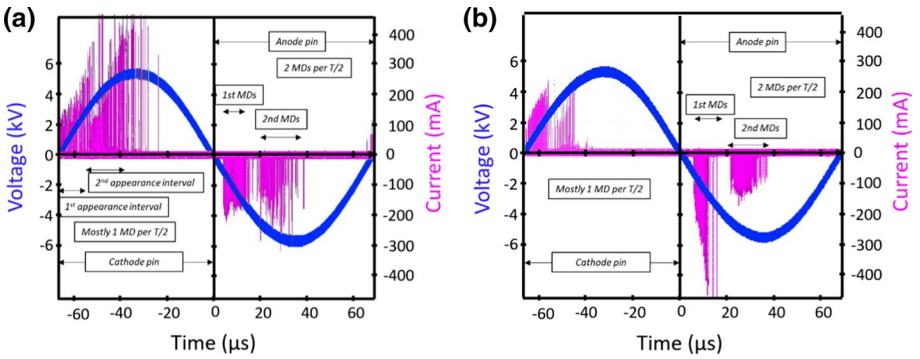

Fig. 2 Current (purple) and voltage (blue) oscillograms after accumulation over 7500 V cycles for **a** dry air without toluene admixture and **b** with admixture of 35 ppm toluene (Color figure online)

significant effects on the discharge dynamics are obtained. For the negative half-cycle still two MD groups appear. The two groups are now separated by a time window of about 6 µs and MDs in the 1st group can exceed amplitudes of 200 mA, while the MDs in the second group are weaker. In the positive half-cycle clearly weaker MDs are obtained if toluene is admixed. In most cycles current pulses with amplitudes in the range 100–200 mA appear in the first or second interval. MD with an amplitude higher than 200 mA are rare.

For 1.5 sccm gas flow admixture the value of toluene concentration was determined at 35 ppm ± 2 ppm by means of micro GC analysis. After about 20 h of operation, the discharge behaviour shown in Fig. 2 b remained when the discharge was operated with dry air. This will be discussed further in "Discussion" section.

The employed multi-dimensional TC-SPC system allows recording of MDs in defined intervals of the applied voltage cycle and, thus, to investigate the discharge development for the two subsequent MDs in case of the anodic pin configuration. The discharge development and the morphology of individual MDs are presented in Fig. 3 by means of ICCD images and TC-SPC results (time-position-photon count plots after an accumulation of 4 h (1.07×10^8 cycles) for SPS and 3 h (8×10^7 cycles) for FNS). As shown in Fig. 3, the discharge development is determined by the positive streamer mechanism. The 1st MD (Fig. 3a) propagates nearly along the central axis between anode tip and dielectric meniscus and spreads on the dielectric surface (see ICCD image). The TC-SPC results show that the streamer inception starts near the pin electrode. After streamer reaches the dielectric surface, the propagation of discharge channels along the gas-dielectric interface is observed and a bulk plasma (so-called anode glow) forms. From 19 ns on the decay of the discharge in the volume is obtained. Due to residual surface charges from the 1st MD, the 2nd MD avoids the centre of the dielectric, and covers the sides of the surface (see Fig. 3b). This influences MD development of the 2nd MD as well, but since the same discharge development is observed in air we refer to our previous contribution [50] and do not discuss the details here.

The small toluene admixture does not affect the breakdown mechanisms. Even the velocities of the streamers in the gap or on the surface are almost the same than in dry air. The decay of the intensity of the FNS and the SPS is unaffected as well. Obviously, the effective lifetime of the excited states is not influenced by the presence of toluene due to its low density compared to nitrogen and oxygen. The rate coefficients for the quenching of the state $N_2(C^3\Pi_u)$ by nitrogen and oxygen are $k^C_{q,N2} = (0.4 - 1.7)\times10^{-11}\mathrm{cm}^3/\mathrm{s}$

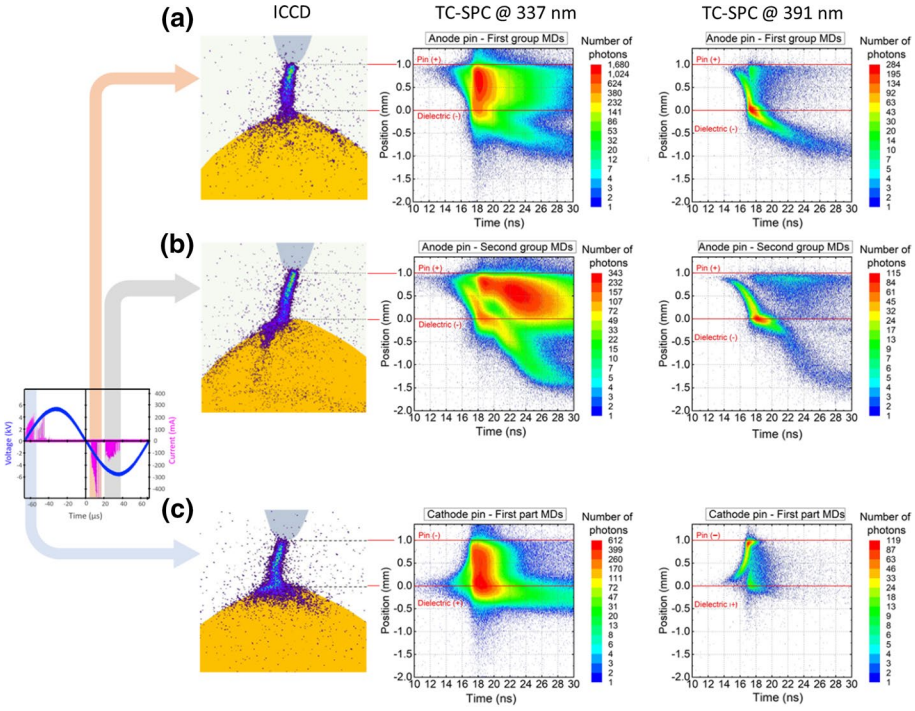

Fig. 3 ICCD photos of individual MDs and spatio-temporally resolved development of the emission of the second positive system of nitrogen (0–0 transition at 337 nm) and first negative system of nitrogen (0–0 transition at 391 nm) for the different time windows of the applied high voltage in dry air with 35 ppm toluene admixture. **a** 1st MD in negative half-cycle (anodic pin); **b** 2nd MDs in negative half-cycle; **c** MDs in the first interval of positive half-cycle. The number of recorded photons is shown in color-coded logarithmic scale (Color figure online)

and $k^C_{q,O2} = (1.9 - 3.3) \times 10^{-10}\text{cm}^3/\text{s}$, respectively [54]. For the state $N_2{}^+(B^2\Sigma^+_u)$ these constants are $k^B_{q,N2} = (1.4 - 9.8) \times 10^{-10}\text{cm}^3/\text{s}$ and $k^B_{q,O2} = (4.4 - 11.0) \times 10^{-10}\text{cm}^3/\text{s}$, respectively [54]. Rate coefficients for the quenching of the states by toluene are not known, but should be in the order of $10^{-4}\text{cm}^3/\text{s}$ to have a significant influence on the effective lifetime under the conditions being considered. The quenching coefficients for the metastable states $N_2(A^3\Sigma^+_u)$ by benzene (C_6H_6) are $k^A_{q,VOC} = (1.6 - 3.2) \times 10^{-10}\text{cm}^3/\text{s}$ [55] and thus, far below this threshold.

In the work [55] the role of the nitrogen metastable molecules on the removal of toluene in nitrogen and nitrogen/oxygen was discussed. Toluene removed efficiently through dissociation processes involving electrons and nitrogen excited species in nitrogen without oxygen. The admixture of oxygen leads to considerable quenching of $N_2(A^3\Sigma^+_u)$. The values for quenching by nitrogen and oxygen are $k^A_{q,N2} = 3.0 \times 10^{-18}\text{cm}^3/\text{s}$ and $k^A_{q,O2} = 3.83 \times 10^{-12}\text{cm}^3/\text{s}$ [56, 57]. Using these values and a radiative lifetime of $\tau_0 = 2\,\text{s}$ its effective lifetime is 50.2 ns in air, and 49.8 ns with toluene. For the metastable $N_2(a'^1\Sigma^-_u)$ the effective lifetime is 0.4 ns in dry air and the effect of toluene admixture is also negligible. These timescales are significantly lower than for other radicals [58] and, for an admixture of oxygen in the range of some volume percent, oxygen and

hydrogen atoms as well as hydroxyl radicals are dominant for the toluene removal [6, 55].

The current pulses of the 1st and 2nd group MD are also not significantly changed when toluene is admixed. The current pulse averaged over 512 cycles for dry air with and without toluene admixture as measured with the current probe are presented in Fig. 4a, b. The timescales are different than the time scale presented in the TC-SPC results as both methods (current pulse oscillography, TC-SPC) are independent from each other. The 1st MD current pulses are characterized by a steep increase and an exponential decay, while the 2nd MD current pulses reach a first local maximum after a steep inset, but then saturates for about 2 ns before a second, the global maximum is reached. From the integration of current pulses over time, taking the values of total and barrier capacitance ($C_{\mathrm{tot}} = 0.21$ pF and $C_{\mathrm{b}} = 0.68$ pF) into account [see Eq. (1)], the dissipated charge is calculated [29]. Without toluene 2.5 nC and 3.8 nC are obtained for the 1st and 2nd MDs, respectively. Admixing toluene increases the value of charge for the 1st MDs (2.9 nC) but reduces the value for the 2nd MDs (3.2 nC).

$$Q_{MD} = \frac{1}{1 - C_{tot}/C_b} \int_{t_1}^{t_2} I(t)dt \tag{1}$$

The MDs for the positive half-cycle (pin acts as the cathode), presented in Fig. 3c, show a similar morphology to the 1st MD in the negative half-cycle, with the difference there are no distinct discharge channels observed on the dielectric surface. The discharge inception starts in front of the anode (dielectric) and a cathode directed ionisation wave followed by bulk plasma formation in the entire gas-gap is observed. Only a limited part of the surface is covered by plasma and there is no distinct propagation on the surface. Again, there is no significant difference to the MDs development observed in air without toluene admixture. Similar current pulses to the 1st MDs in the negative half-cycle are obtained, i.e. a steep increase followed by slower decay (see Fig. 5a, b). Due to reversed polarity, the sign of the current changed to positive values. MDs appearing at the very beginning of the half-cycle (1st appearance time interval in Fig. 2b) have a longer duration in dry air. MDs in the 2nd appearance time interval (no

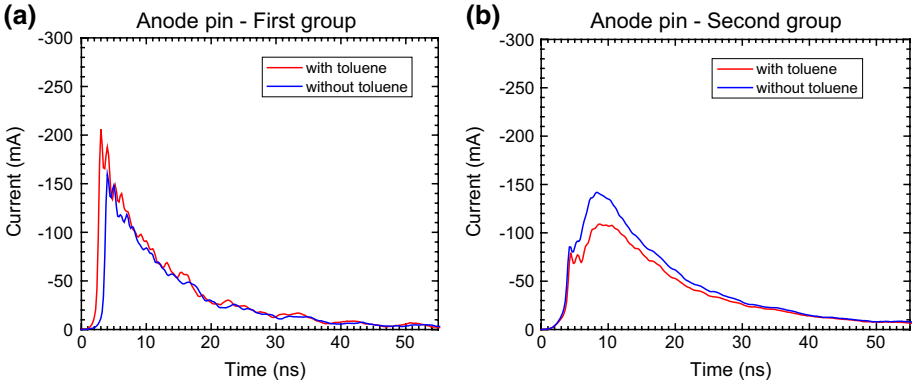

Fig. 4 Current pulses measured with current probe CT-1 for the negative half-cycle. Results after averaging over 512 events (Color figure online)

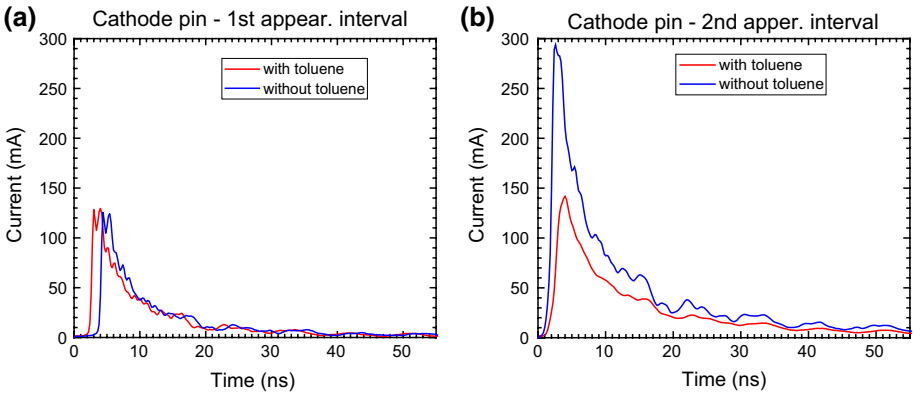

Fig. 5 Current pulses measured with current probe for positive half-cycle. Results after averaging over 512 high voltage cycles (Color figure online)

TC-SPC results shown because of seldom events) are longer (50 ns instead of 30 ns) than in the 1st interval, and the current increase is less steep (about 5 ns instead of 2 ns). Without the toluene admixture, much higher current pulses (280 mA amplitude in the mean, but up to 700 mA for individual MDs) can be obtained (see "Microdischarge Inception and Dynamics" section). The corresponding values of mean dissipated charge in the 1st interval are 1.5 nC no matter if toluene is admixed or not. The main difference is observed in the second interval, where the high current MDs appear. Here, the dissipated charge value become significantly smaller (2.5 nC instead of 4.1 nC).

Microdischarge Inception and Dynamics

As seen in the previous subsection, the admixture of toluene to dry air does not change the MD development but it effects the overall discharge dynamics. For the negative

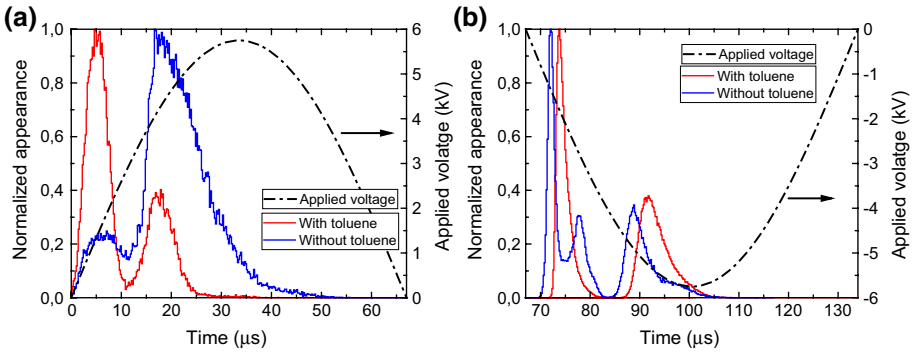

Fig. 6 Normalized appearance (pulse distribution function) of the MD current pulses within one period T of high voltage for dry air with and without toluene admixture; **a** cathode pin with mostly on MD per T/2; **b** anode pin with two subsequent MDs (Color figure online)

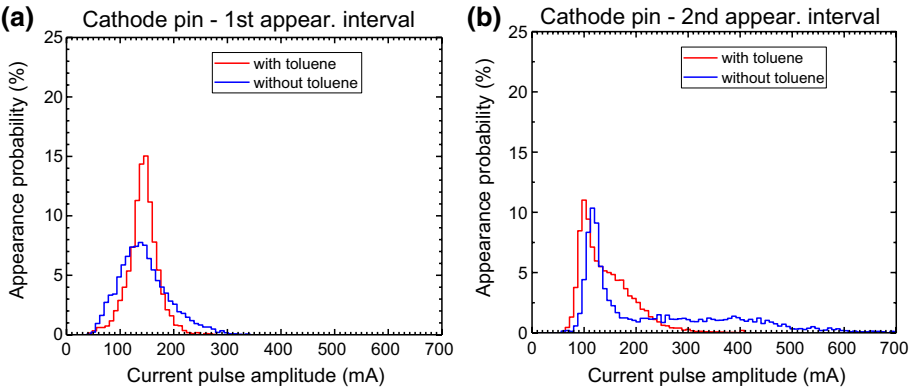

Fig. 7 Distribution of the current pulse amplitudes within the positive half-cycle (cathode pin) of the applied voltage (Color figure online)

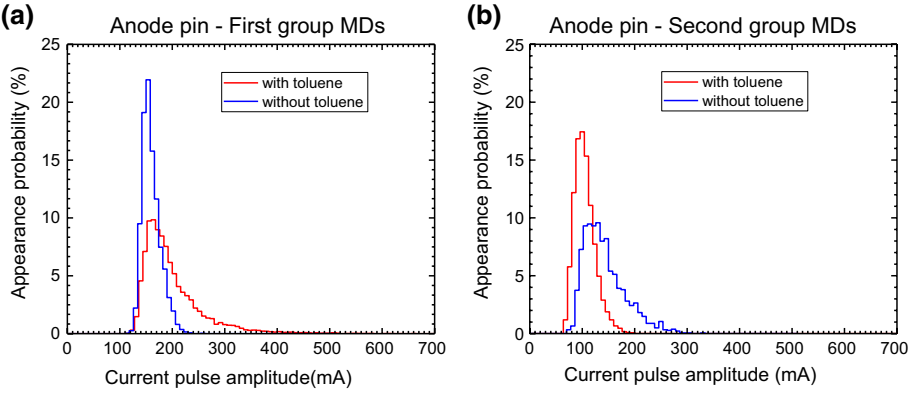

Fig. 8 Distribution of the current pulse amplitudes within the negative half-cycle (anode pin) of the applied voltage (Color figure online)

half-cycle the difference of dissipated charge is about 20%, but for positive half cycle, MDs with a higher amplitude are supressed at the same high voltage when toluene is admixed. This behaviour is further analysed by means of averaged electrical measurements. Figure 6 shows the normalized appearance of MD current pulses (pulse distribution function), while Figs. 7 and 8 present the distribution of current pulse amplitudes for each of the sections.

The highest probability to detect a MD in the air-toluene gas mixture in the positive half-cycle is within the first 10 µs after the zero crossing of the high voltage (see Fig. 6a). Without toluene, the tendency is that MDs are ignited later and more distributed over the phase of the high voltage. The pulses in the first interval have a most probable amplitude of about 150 mA, but spread over a range of 44–250 mA (see Fig. 7a). The spreading of amplitudes is even larger in the second interval (Fig. 7b). In this interval, the most probable amplitude is slightly higher for pure air compared to the one with toluene admixture, and even amplitudes of up to 600 mA are reached. For the negative half-cycle (anodic pin) the

toluene admixture causes higher current pulses in case of the 1st group MDs (Fig. 8a), but lower amplitudes of the 2nd group (Fig. 8b).

The mean energy per MD E_{MD} can be calculated by multiplying the values of charge from the average current pulses Q_{MD} (Figs. 4, 5) with the value of the voltage at the breakdown V_{bd} [Eqs. (2, 3)] [30]. This value is assumed as constant during the MD development in case of sinusoidal operation in the kHz-range. It cannot be determined directly from the electrical measurements in our particular case due to the erratic behaviour of the discharge. However, from the normalised appearance histograms in Fig. 6b it is seen that the external voltage V_{appl} (in the mean) needs to increase by (3.5 ± 0.6) kV to start the 2nd MD. Thus, this value is needed for the ignition of a MD. Therefore, it is assumed as an estimation for the inception voltage. Considering the voltage drop over the barrier, which is calculated with the capacities of barrier and discharge arrangement, the value of V_{bd} is about (2.4 ± 0.4) kV. This value is applied for both polarities. The corresponding value of the reduced electric field for electrical breakdown is (90 ± 15) Td and in fair agreement with the known Paschen-values for air. The measured mean charges, resulting MD energies and mean power is given in Table 1.

With and without toluene admixture, nearly similar values of E_{MD} are obtained for the negative half cycle as well as the first interval in the positive half-cycle. In the second interval, a higher energy is dissipated in case of air. Taking the probabilities of discharge appearance per section p into account (for positive polarity it is calculated from the data in Fig. 7), the mean dissipated power $\bar{P}$ in case of air is about (178 ± 31) mW, while for toluene admixture a considerably smaller value, namely (138 ± 24) mW, is calculated (Eq. (4)). Considering the gas flow value, the specific energy input of the discharge with toluene admixture is about (27 ± 5) J/L, and (36 ± 6) J/L in air. The difference in the power consumption is due to the fact, that (1) the dissipated charge in the MDs appearing in the 2nd interval of cathodic pin half-cycle drops with toluene admixture (2.5 instead of 4.1 nC), and, (2) these stronger MDs appear less frequent. This is also clearly seen in the amplitude distributions in Fig. 8a, b. Except the 1st group MDs in negative polarity there is always the tendency to higher current pulse amplitudes in air without the admixture. The most significant effect is obtained in the 2nd interval of the positive half-cycle (see Figs. 6, 7b).

$$E_{MD} = Q_{MD} V_{bd} \tag{2}$$

Table 1 Overview of mean charge Q_{MD} (by integration of average current pulses), mean energy per MD E_{MD} and mean power per section $\bar{P}$

Gas	Polarity	Interval	Mean charge Q_{MD} (nC)	Energy E_{MD} (µJ)	Probability p (−)	Power $\bar{P}$ (mW)
Air	Negative	1st group	2.5	6. ± 1.0	1	178 ± 31
		2nd group	3.8	9. ± 1.6	1	
	Positive	1st interval	1.5	3. ± 0.6	0.19	
		2nd interval	4.1	9. ± 1.7	0.81	
Air + tol.	Negative	1st group	2.9	7. ± 1.2	1	138 ± 24
		2nd group	3.2	7. ± 1.3	1	
	Positive	1st interval	1.5	3.5 ± 0.6	0.72	
		2nd interval	2.5	6.1 ± 1.0	0.18	

The probabilities of the corresponding discharge event are also given. In case of negative polarity two MDs per T/2 appear (thus probability is 1 for each group), in case of positive polarity one MD per T/2 appears (sum of both probabilities are equal to 1)

$$V_{bd} = \left(1 - {}^{C_{tot}}/_{C_b}\right) V_{appl}|_{t=t_b} \tag{3}$$

$$\bar{P} = f \cdot \sum_i (E_{MD,i} \cdot p_i) \tag{4}$$

It must be mentioned that the values in Table 1 are based on averaged measurements (in particular for Q_{MD}). A more precise analysis would require the determination of the charge and the breakdown voltage for individual MD current pulses followed by statistical methods. This was not in the focus of this study.

The effect of inlet concentration of toluene and temperature on the energy per MDs generated in a pulsed DBD was investigated in [59]. The energy dissipated per pulse was in the range 4.4–5.3 mJ and only a slight increase with the concentration was measured. Due to operation with fast increasing high voltage pulses and a different reactor design, the values in [55, 59] are about three orders of magnitude higher. The small increase of the energy per pulse was related to an increase of oxygen atom production and thus, a decrease of the toluene removal rate. Overall, changes in the discharge physical characteristics over time did not improve the toluene removal efficiency. A similar trend than in [59] is seen here only for the 1st group MDs, but not for the other MDs. This is related to the different MD development within the high voltage cycle (shown by the TC-SPC results).

Discussion

To discuss the obtained effect of the toluene admixture on the MDs properties and their inception dynamics three hypotheses are considered: (1) influence on the inception voltage by additional ionization mechanisms and volume memory effects, (2) toluene decomposition reactions, and (3) modification of the surface of the electrodes by plasma treatment.

As mentioned in "Experimental Set-Up" section, to obtain comparable results for both gas compositions, the same voltage amplitude (11.4 kV_{pp}) was used in all experiments. However, it was observed that the effect of toluene admixture on the distribution of the current pulses over the applied voltage cycle is similar to applying higher voltages (overvoltage) in pure air (14.5 kV_{pp}). Furthermore, a lower voltage amplitude (10.5 kV_{pp}) is needed for the stable operation of the discharge with the toluene admixture, while for dry air 11.4 kV_{pp} is required (i.e. 300 V less gap voltage value). Thus, toluene admixture seems to decrease the value of ignition voltage slightly. Consequently, MDs are generated at lower gap voltage than in air, which results in lower current amplitudes. The difference of the ignition voltage is within the error bar of the value used for V_{bd} in Table 1.

The ionization energy of toluene (8.8 eV) is significantly lower than for molecular oxygen (12.1 eV) and nitrogen (15.6 eV). Penning ionisation by nitrogen metastable molecules cannot explain a lower breakdown voltage in this gas mixture. The energies of $N_2(A)$ (6.16 eV) and $N_2(a')$ (8.4 eV) are not sufficient to ionise toluene. Another possibility is Penning ionisation of by-products of toluene decomposition. However, at the low specific input energies (27 J/L) the overall conversion is about 20% [52] and effective lifetimes of the metastable nitrogen molecules are low due to quenching by oxygen (see "Microdischarge Morphology and Development" section).

The electron-impact ionization cross section of toluene has not only a lower threshold energy than the cross sections for nitrogen and oxygen, also the values are significantly

higher. At an electron energy of 15 eV its value is about 2.4×10^{-16} cm^2 [60, 61] for toluene, but 1×10^{-17} cm^2 for oxygen and zero for nitrogen [62]. The maximum ionization cross section of toluene is at 60 eV with a value of 1.5×10^{-15} cm^2, while about 2.5×10^{-16} cm^2 at 100 eV for nitrogen as well as oxygen. Thus, rate coefficients for electron impact ionization in weakly ionized non-thermal plasmas ($T_e \approx 1$ eV) will be considerably larger for toluene.

Toluene is detectable by Atmospheric Pressure Chemical Ionization (APCI) with a sensitivity in the sub-ppb (parts-per-billion) range [63, 64]. APCI utilises DC corona discharges for the formation of primary ions, which start reaction cascades leading to radical and molecular cations, protonated clusters and other ion–molecule complexes. These are then detected by a mass spectrometer. A study of the ions being formed by APCI in dry air concluded that in case of negative DC-polarity the same kind of ions were produced in both dry and toluene-polluted air [65]. But, in positive DC-polarity different ions than in air were formed. Exothermic charge- and proton transfer ion–molecule reactions between toluene and O_2^+, N_2^+ and H_3O^+ led to the generation of $C_7H_8^+$, $[C_7H_8+H]^+$ and their ion–molecule complexes, e.g. $C_7H_8^+(C_7H_8)$. The rate coefficients for these formation processes are in the range of 10^{-9} cm/s. The same ions and rate coefficients have also been investigated for a pulsed electron beam at low pressure [66]. Since these ions are bigger and heavier than O_2^+ and N_2^+, their mobility is smaller. The ion mobility in dry air with and without toluene admixture was determined in the same work in DC corona discharges by means of current–voltage measurements in a wire-to-cylinder reactor. The concentration of toluene was 500 ppm, and DC high voltage (positive or negative polarity) was applied to the wire electrode. The Townsend formula was used to determine the ion mobility of positive ions, which was 2.35 cm^2 V^{-1} s^{-1} for pure air and 1.79 cm^2 V^{-1} s^{-1} for toluene-containing air. In correlation with this result, the current–voltage characteristics were almost identical in negative polarity (wire as cathode) while in positive (wire as anode) the presence of toluene produced a smaller discharge current when compared to dry air. The authors [65] conclude that ionic reactions could be responsible for the initial stages of the toluene removal process in case of positive DC corona discharges.

In our experiment subsequent "switching" between both polarities is present. The effect on the discharge is more significant when the (albite grounded) pin electrode acts as the cathode. This is somewhat different compared to the results of the DC corona measurements in [65]. However, the formation of ions with lower mobility in the MDs in the negative half-cycle (anodic pin) could lead to a higher residual volume charge at the start of the following positive half-cycle. This could also explain the lower inception voltage obtained with the toluene admixture. In case of air, residual volume charge is lower at the start of the positive half-cycle. Consequently, it is more probable that the MDs appear in later phases of the applied voltage and thus, have higher current pulse amplitudes. It is known for pulsed single DBDs in N_2 with small admixtures of O_2 that sufficient pre-ionization can affect the breakdown leading to weaker MDs [30]. The formation of low-mobility ions is therefore a candidate to explain the suppression of the high-current MDs by the toluene admixture. This also influences the MDs inception in the following (i.e. negative half-cycle). Since weak MDs are more probable, the amount of deposited surface charge on the dielectric surface is lower and so it is the electric memory field after the voltage reversal (zero crossing). This explains why 1st group MDs appear later within the half-cycle if toluene is present (Fig. 7b). Since the applied voltage value is higher when these MDs ignite, they have higher current pulse amplitudes (160 mA most probable amplitude within a range of 130 mA up to 400 mA, see Fig. 8a). A quantitative proof of this hypothesis, and

whether chemi-ionization or associative ionization play a role, remains as an open question for further studies.

Toluene as a molecule consisting of an aromatic ring with six carbon and five hydrogen atoms as well as a methyl group ($–CH_3$) can also be dissociated or vibrational/rotationally excited by electron collisions. These processes consume high-energy electrons. According to decomposition pathway studies conducted with GC–MS analysis (see [5, 6, 55]) oxygen radicals, but also energetic electrons are the most important species for toluene removal. The analysis of organic by-products of toluene removal suggest H-abstraction from the methyl group by both electrons and O or OH radicals as the primary destruction pathway. The subsequent reactions lead to the formation of various partially oxidized intermediates, which finally convert to CO_2 and H_2O. These reactions can also be induced by electron collisions. In summary, the toluene destruction mechanisms consumes energetic electrons, which leads to a decrease of measured dissipated energy. The effect of the toluene admixture on the average charge is not significant, but in most cases lower current amplitudes are obtained than in air.

As mentioned before the discharge dynamics reported in Fig. 2 b remained when the discharge cell was operated in dry air after about 20 h (i.e. after time-consuming TC-SPC and ICCD measurements). This is a clear indication that surface processes must be considered. During the experiments with 35 ppm toluene admixture the current signals were continuously inspected and the discharge behaviour did not changed during this period. However, after the measurements a brownish, non-wipeable layer was found on the barrier electrode. A similar observation was reported in [55, 67]. It was explained by the deposition of polymer layers on the dielectric due to plasma polymerization. After polishing the barrier electrode with fine sandpaper the discharge behaviour was as expected for air (Fig. 2a), but after some hours of operation with dry air, the discharge behaviour changed to the regime similar to Fig. 2b. This suggest, that toluene (and other hydrocarbons) are deposited on the cell walls (made of polycarbonate), and evaporated and diffused into the plasma zone, where it can cause change of discharge behaviour and new polymer layers on the surface of the electrodes.

Obviously, the surface layer does not influence the MD morphology as seen by comparing the ICCD camera pictures (see Fig. 3 and ICCD images in [50]). The spreading of the MD foot and the size of the surface spot are about the same. Also, the values of dissipated charge change only slightly. These observations suggest a minor effect on the MD properties by the deposited layer, but a comprehensive investigation of this subject remains for future work.

Conclusions and Outlook

The properties, the inception dynamics and the development of MDs in toluene containing dry air are studied in an asymmetric DBD arrangement consisting of a metal pin and a hemispherical dielectric-covered electrode. The discharge is operated by sinusoidal high voltage with a frequency of 7.5 kHz. Several discharge events are obtained within one high voltage cycle.

It is shown that small concentration of toluene (up to 35 ppm) has only minor effects on the discharge physics. The MD development is similar to that in dry air (positive streamer mechanism), only the inception dynamics and the properties of MDs change by the toluene admixture. The toluene admixture affects the dissipated charge and energy of MDs only

slightly and there is no distinct trend obtained in the discharge geometry being considered. The main influence of toluene is the suppression of high current MDs in the positive half-cycle of the applied voltage (the pin acts as the cathode). In addition, the minimum applied voltage to operate the plasma is lower with 35 ppm toluene admixture (about 300 V). Possible explanations are higher rate coefficients for electron impact ionization of toluene, additional ionization processes and the formation of toluene-ion complexes with a lower mobility than nitrogen and oxygen ions. These ions could be responsible for a volume memory space charge, which affect the MD properties and supress the formation of the high current MDs. Furthermore, toluene decomposition reactions consume energetic electrons. Also observed is the modification of the surface by plasma treatment. The effect on MD properties and inception dynamics is not found to be significant, but a comprehensive statement cannot be done without further studies dedicated to this issue. Such studies must include a variation of the toluene concentration (including higher admixtures) as well as a coupling with high-sensitive gas-analysis in order to correlate physical and chemical effects. An in situ surface analysis would enable the study of the influence of surface modification.

The asymmetric electrode arrangement was chosen as a representation of the conditions in DBD reactors used for studying pollutant degradation. According to [59] it is preferable to use discharge pulses with a highest energy per pulse and less number of pulses in order to obtain optimal removal. Simulation results in [68] suggest that a maximized area density of MDs will most likely lead to an optimum removal efficiency (studied for nitrogen oxides conversion from automotive exhausts). In [69] it is suggested that treatment of a volume element of the gas with a series of discharge pulses with a smaller energy deposition is more efficient than treating the gas with a single pulse of high energy deposition. These examples demonstrate the highly complex interaction of discharge physics and energy distribution, and the chemistry. And, it gives plenty of room for optimization.

Here, we show that microdischarges generated in the same half-cycle of the high voltage can be different and that they influence events in the following half-cycle. More statements on the role of residual ions and surface modifications require an experiment in a symmetric arrangement and only one MD per half-cycle. This remains for future studies, as well as the simulation of DBDs in VOC containing gases. Such investigations would also be interesting with catalytic barrier materials in order to characterize the interaction between plasma and surface from physics and chemistry viewpoints.

Acknowledgements The work was supported by Deutsche Forschungsgemeinschaft (DFG) under Grant BR 4133/4-1.

References

1. Rafflenbeul R (1998) Müll Abfall 1:38–44
2. Thevenet F, Sivachandiran L, Guaitella O, Barakat C, Rousseau A (2014) J Phys D Appl Phys 47:224011
3. Kim HH (2004) Plasma Process Polym 1:91–110

4. Magureanu M (2012) VOC removal from air by plasma-assisted catalysis—experimental work. In: Parvulescu VI, Magureanu M, Lukes P (eds) Plasma chemistry and catalysis in gases and liquids. Wiley-VCH, Weinheim, pp 131–170
5. Vandenbroucke AM, Morent R, De Geyter N, Leys C (2011) J Hazard Mater 195:30–54
6. Vandenbroucke AM, Morent R, De Geyter N, Leys C (2012) J Adv Oxid Technol 15:232–241
7. Xiao G, Xu W, Wu R, Ni M, Du C, Gao X, Luo Z, Cen K (2014) Plasma Chem Plasma Process 34:1033–1065
8. Magureanu M, Dobrin D, Mandache NB, Cojocaru B, Parvulescu VI (2013) Front Chem 1(7):1–6
9. Jia Z, Wang X, Foucher E, Thevenet F, Rousseau A (2018) Catalysts 8:303
10. Kogelschatz U (2002) IEEE Trans Plasma Sci 30:1400–1408
11. Kogelschatz U (2003) Plasma Chem Plasma Process 23:1
12. Becker KH, Kogelschatz U, Schoenbach K, Barker R (2004) Non-equilibrium air plasmas at atmospheric pressure. CRC Press, Boca Raton
13. Becker KH, Schoenbach KH, Eden JG (2006) J Phys D Appl Phys 39:R55–R70
14. Becker KH (2018) Plasma Phys Technol 5(1):5–9
15. Bruggeman P, Brandenburg R (2013) J Phys D Appl Phys 46:464001
16. Laroussi M, Lu X, Keidar M (2017) J Appl Phys 122:020901
17. Eliasson B, Hirth M, Kogelschatz U (1987) J Phys D Appl Phys 20:1421–1437
18. Falkenstein Z, Coogan JJ (1997) J Phys D Appl Phys 30:817
19. Heuser C, Pietsch, G (1985) In: Timmermans (ed) Proceedings of the 7th International symposium on plasma chemistry, Eindhoven, pp 321–326
20. Laroussi M, Lu X, Kolobov V, Arslanbekov R (2004) J Appl Phys 96:3028–3030
21. Celestin S, Bonaventura Z, Guaitella O, Rousseau A, Bourdon A (2009) Eur Phys J Appl Phys 47:34–39
22. Akishev YS, Demyanov A, Karalnik V, Monich A, Trushkin N (2003) Plasma Phys Rep 29:82–91
23. Peeters FJJ, van de Sanden MCM (2015) Plasma Sour Sci Technol 24:015016
24. Šimek M (2014) J Phys D Appl Phys 47:463001
25. Šimek M, Prukner V, Schmidt J (2011) Plasma Sour Sci Technol 20:025009
26. Volk G (1992) Zeitaufgelöste Bestimmung von Plasmaparametern der stillen Entladung in Stickstoff. Dissertation University of Stuttgart
27. Starikovskaia SM, Allegraud K, Guaitella O, Rousseau A (2010) J Phys D Appl Phys 43:124007
28. Stepanyan SA, Soloviev VR, Starikovskaia SM (2014) J Phys D Appl Phys 47:485201
29. Liu Ch, Fridman A, Dobrynin D (2019) J Phys D Appl Phys 52:105205
30. Kettlitz M, Höft H, Hoder T, Reuter S, Weltmann K-D, Brandenburg R (2012) J Phys D Appl Phys 45:245201
31. Kozlov KV, Wagner H-E, Brandenburg R, Michel P (2001) J Phys D Appl Phys 34:3164–3176
32. Hoder T, Brandenburg R, Basner R, Weltmann K-D, Kozlov KV, Wagner H-E (2010) J Phys D Appl Phys 43:124009
33. Brandenburg R (2017) Plasma Sour Sci Technol 26:053001
34. Lukas C, Spaan M, Schulz-von der Gathen V, Thomson M, Wegst R, Döbele HF, Neiger M (2001) Plasma Sour Sci. Technol. 10:445
35. Dilecce G (2014) Plasma Sour Sci Technol 23:015011
36. Nemschokmichal S, Meichsner J (2013) Plasma Sour Sci Technol 22:015006
37. Ono R (2016) J Phys D Appl Phys 49:083001
38. Braun D, Gibalov VI, Pietsch GJ (1992) Plasma Sour Sci Technol 1:74–89
39. Gibalov VI, Pietsch GJ (2000) J Phys D Appl Phys 33:2618
40. Pietsch GJ, Gibalov VI (2012) Plasma Sour Sci Technol 21:024010
41. Yurgelenas YV, Wagner H-E (2006) J Phys D Appl Phys 39:4031–4043
42. Steinle G, Neundorf D, Hiller W, Pietralla V (1999) J Phys D Appl Phys 32:1350–1356
43. Eliasson B, Egli W, Kogelschatz U (1994) Pure Appl Chem 66:1275–1286
44. Xu XP, Kushner M (1998) J Appl Phys 83:7522–7532
45. Boeuf JP, Lagmich Y, Unfer T, Callegari T, Pitchford LC (2007) J Phys D Appl Phys 40:652–662
46. Sakiyama Y, Graves DB, Chang H-W, Shimizu T, Morfill GE (2012) J Phys D Appl Phys 45:425201
47. Falkenstein Z (1999) J Appl Phys 85(1):525–529
48. Massines F, Rabehi A, Decomps P, Ben Gadri R, Segur P, Mayox C (1998) J Appl Phys 28:2950
49. Lovascio S, Blin-Simiand N, Magne L, Joran F, Pasquiers S (2015) Plasma Chem Plasma Process 35:279
50. Jahanbakhsh S, Brüser V, Brandenburg R (2018) Plasma Sour Sci Technol 27:115011
51. Müller S, Zahn RJ (2007) Contrib Plasma Phys 47:520–529
52. Schmidt M, Schiorlin M, Brandenburg R (2015) Open Chem 3:477–483

53. Bilek P, Obrusnik A, Hoder T, Simek M, Bonaventura Z (2018) Plasma Sour Sci Technol 27:085012
54. Obrusnik A, Bilek P, Hoder T, Simek M, Bonaventura Z (2018) Plasma Sour Sci Technol 27:085013
55. Blin-Simiand N, Jorand F, Magne L, Pasquiers S, Postel C, Vacher J-R (2008) Plasma Chem Plasma Process 28:429–466
56. Guerra V, Sa PA, Loureiro N (2004) J Phys D Appl Phys 34:1745–1755
57. Kossyi A, Kostinsky AY, Matveyev AA, Silakov VP (1992) Plasam Sour Sci Technol 1:207–220
58. Rudolph R, Francke K-P, Miessner P (2002) Plasma Chem Plasma Process 22:401–412
59. Pasquiers S, Heninger M, Blin-Simiand N, Lemaire J, Bauville G, Bournonville B, Louarn E, Jorand F, Mestdagh H (2018) J Phys D Appl Phys 51:425201
60. Vacher JR, Jorand F, Blin-Simiand N, Pasquiers S (2007) Chem Phys Lett 434:188–193
61. Harrison AG, Jones EG, Gupta SK, Nagy GP (1966) Can J Chem 44(16):1967–1973
62. National Institute of Standards and Technology (NIST) Gaithersburg, USA: Electron impact cross sections ionization and excitation database. https://www.nist.gov/pml/electron-impact-cross-sections-ionization-and-excitation-database
63. Terrier P, Desmazieres B, Tortajada T, Buchmann W (2011) Mass Spectrom Rev 30:854–874
64. Huang G, Gao L, Duncan J, Harper JD, Sanders NL, Ouyang Z, Cooksa RG (2010) J Am Soc Mass Spectrom 21:132–135
65. Schiorlin M, Marotta E, Rea M, Paradisi C (2009) Environ Sci Technol 43:9386–9392
66. Sieck LW, Buckley TJ, Herron JT, Green DS (2001) Plasma Chem Plasma Process 21:441–457
67. Mista W, Kacprzyk R (2008) Catal Today 2008(137):345–349
68. Doraj R, Kushner MJ (2013) J Phys D Appl Phys 36:1075–1083
69. Doraj R, Kushner MJ (2001) J Phys D Appl Phys 34:574–583